

# Strange Hadron Production at High Baryon Density

Hongcan Li<sup>1,2,\*</sup> (for the STAR collaboration)

<sup>1</sup>Central China Normal University, Wuhan 430079, China

<sup>2</sup>University of Chinese Academy of Sciences, Beijing 101408, China

**Abstract.** Strange hadrons have been suggested as sensitive probes of the properties of the nuclear matter created in heavy-ion collisions. At few-GeV collision energies, the formed medium is baryon-rich due to baryon stopping effect. In these proceedings, the recent results on strange hadron production in Au+Au collisions at  $\sqrt{s_{NN}} = 3.2, 3.5, 3.9$  and 4.5 GeV with the fixed-target mode from the STAR Beam Energy Scan (BES) phase-II program will be presented. The transverse momentum spectra, rapidity density distributions, excitation function and centrality dependence of strange hadrons ( $K_S^0$ ,  $\Lambda$ ,  $\Xi^-$ ) are shown. These results will be compared with those from higher collision energies and physics implication will be discussed by comparing to the transport model calculations.

## 1 Introduction

Relativistic heavy-ion collisions provide an excellent opportunity to study quark-gluon plasma (QGP). Searching for quantum chromodynamics (QCD) critical point, studying properties of QGP and exploring QCD phase diagram are major physical goals of the STAR experiment. Therefore, the BES program was developed at Relativistic Heavy-Ion Collider (RHIC). In BES-II program, by fixed-target (FXT) mode, the collision energy of per nucleon pair in Au+Au collision reach down to 3 GeV, where the baryon chemical potential of the created nuclear matter reaches 750 MeV. Properties of the collision system at the high baryon density may be different compared to the quark gluon plasma where partonic interactions dominate.

Hadrons containing  $s$  and/or  $\bar{s}$  quarks are called strange hadrons. In the initial state of heavy-ion collision, there are no strange hadrons in the collision system, so all the strange hadrons in the final state of heavy-ion collision are produced by the collision process, which indicates that the production mechanism of strange hadrons is highly correlated to the reaction mechanism governing the hadronic collision [1–4]. At the STAR FXT energies, strange hadrons are produced near or below the threshold energy, then their yields, especially the excitation function of multi-strange (anti-)hyperons, may provide strong constraints on the equation-of-state (EoS) of the created medium in the heavy-ion collisions.

## 2 Experimental and data analysis

In BES-II program, STAR detector upgraded its inner Time Projection Chamber (iTTPC), end-cap Time of Flight (eTOF), which enlarge the detector acceptance and improve particle

---

\*e-mail: lihc@mails.cnu.edu.cn

37 identification capabilities. In BES-II program, the STAR experiment collected approximately  
 38 10 more times collision events than BES-I, which ensured that we can perform more accurate  
 39 measurements.

40 In this analysis, we used the dataset of Au+Au collisions at  $\sqrt{s_{NN}} = 3.2, 3.5, 3.9$  and  $4.5$   
 41 GeV. TPC and TOF detectors are used for particle identification and to obtain pure daughter  
 42 for short-lived particle reconstruction. The strange hadrons  $K_S^0, \Lambda$  and  $\Xi^-$  are reconstructed  
 43 by using the hadronic decay channels:  $K_S^0 \rightarrow \pi^+ + \pi^-$ ,  $\Lambda \rightarrow p + \pi^-$  and  $\Xi^- \rightarrow \Lambda + \pi^-$ . The  
 44 KFParticle Finder package is used for the strange hadron reconstruction process [5].

### 45 3 Results and discussions

#### 46 3.1 Transverse momentum spectra and rapidity density distribution

47 In Fig.1, we show the transverse momentum ( $p_T$ ) spectra of  $K_S^0, \Lambda$  and  $\Xi^-$  in Au+Au  
 48 collision at centrality 0-10%. Thanks to the large acceptance of the STAR detector and FXT  
 49 mode setup, we can measure almost the full rapidity range from beam backward rapidity to  
 50 middle rapidity. Because the measured  $p_T$  range cannot reach down to 0, we use different  
 51 functions to fit the data for extrapolation to the unmeasured region. The blast-wave function  
 52 is used to fit  $K_S^0$  and  $\Lambda$ , while the  $m_T$ -exponential function is used to fit  $\Xi^-$ .

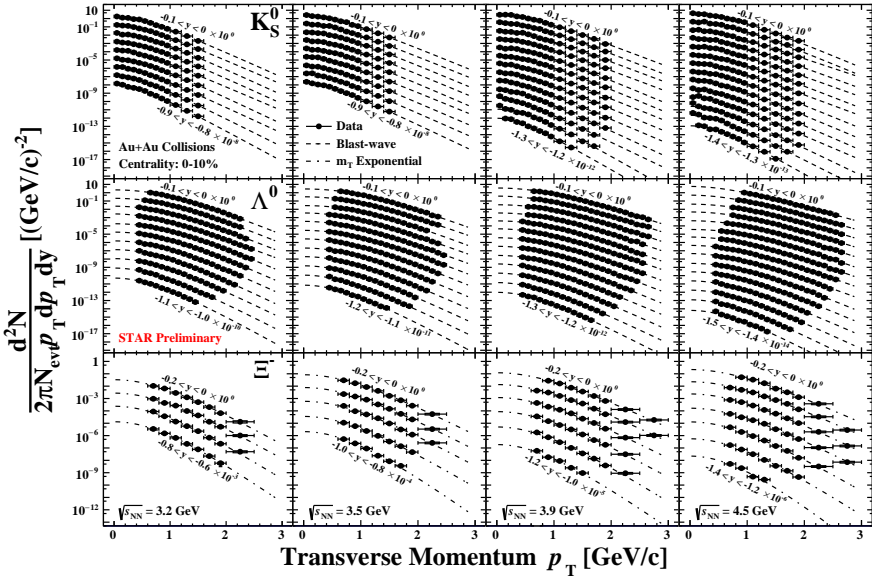


**Figure 1.** Transverse momentum spectra of  $K_S^0, \Lambda$  and  $\Xi^-$  in Au+Au central collision (0-10%) at  $\sqrt{s_{NN}} = 3.2, 3.5, 3.9$  and  $4.5$  GeV. The black solid circles is the measured data points. The dash line is fitting result of blast-wave or  $m_T$ -exponential function.

53 In Fig.2, we show the rapidity density distribution ( $dN/dy$ ) of  $K_S^0, \Lambda$  and  $\Xi^-$  in Au+Au  
 54 collision at centrality 0-10%. They are obtained by integrating the  $p_T$  spectra with measured  
 55 data points and fitting extrapolation function. We observe that the strange hadron yields  
 56 increases as the collision energy grow in these energy range. The  $dN/dy$  shape plateaus at  
 57 mid-rapidity and is gaussian-like at backward rapidity. In order to describe the  $dN/dy$  shape,  
 58  $dN/dy \propto \frac{1}{\text{Cosh}(y^2/\sigma^2)}$  is chosen and used for fitting data points.

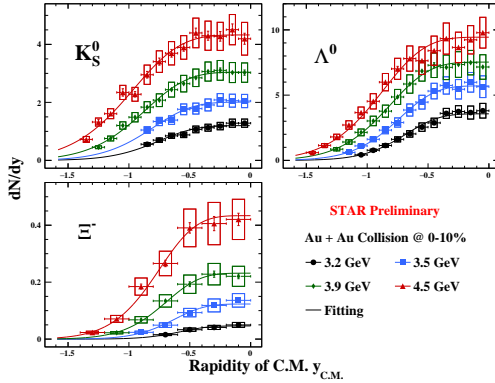


**Figure 2.** Rapidity distribution of  $K_S^0$ ,  $\Lambda$  and  $\Xi^-$  in Au+Au central collision (0-10%) at  $\sqrt{s_{NN}} = 3.2, 3.5, 3.9$  and  $4.5$  GeV. The vertical line is the statistical uncertainties, and the box is the systematic uncertainties.

### 3.2 Strangeness excitation function

Based on above measured results, we can calculate excitation function, which is middle rapidity yield of per average participating nucleon number  $\langle N_{\text{part}} \rangle$  as a function of collision energy, and  $\langle N_{\text{part}} \rangle$  is estimated by Glauber model. In Fig.3, we show the excitation function in Au+Au central collision.

The STAR-FXT energies crossed NN collision threshold energy of  $\Xi^-$  production, so we can see the  $\Xi^-$  yield increases rapidly near the threshold. The rate of increase decreases as the collision energy moves away from the threshold, and approximately remains constant at  $\sqrt{s_{NN}} \sim 20$  GeV or higher. We observe that the  $K_S^0$  and  $\Lambda$  yields cross at  $\sim 8$  GeV, and below the 8 GeV,  $K_S^0$  is less than  $\Lambda$ . This phenomenon indicates that there exists the transition between the baryon-dominated and meson-dominated. The enhancement in baryon yield relative to meson at low energies is likely driven by stronger baryon stopping in the few-GeV energy region.

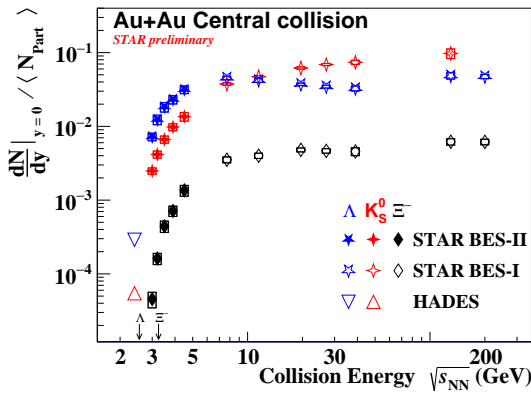


**Figure 3.** Excitation function of  $K_S^0$ ,  $\Lambda$  and  $\Xi^-$  in Au+Au the most central collision. The solid points is STAR BES-II FXT-mode results and the open points is STAR BES-I and HADES results[6–9]. The NN collision threshold energies of  $\Lambda$  and  $\Xi^-$  are marked by two arrows at lower left of figure.

### 3.3 Scaling property of centrality dependence

In order to quantitatively describe the centrality of heavy-ion collisions, we select  $\langle N_{\text{part}} \rangle$  to represent centrality of collision. We use the power law function fitting to get the scaling parameter  $\alpha_S$ , so the scaling parameter  $\alpha_S$  is extracted to represent the centrality dependence of yield.

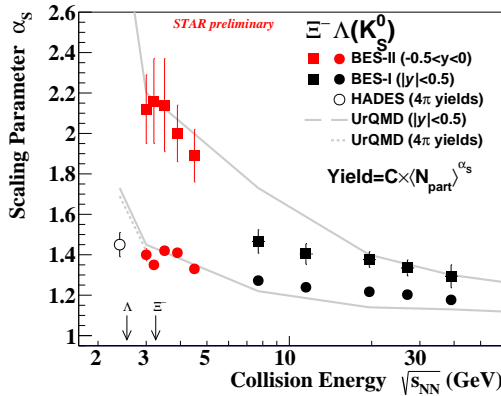


**Figure 4.** Scaling parameter  $\alpha_S$  of  $K_S^0$ ,  $\Lambda$  and  $\Xi^-$  as a function of collision energy. The gray line is the simulation result of the transport model UrQMD.

77 In Fig.4, we show the scaling parameter of  $K_S^0$ ,  $\Lambda$  and  $\Xi^-$  as a function of collision energy.  
78 Single strange hadron production  $K_S^0$  and  $\Lambda$  is associated production via  $NN \rightarrow NAK$ , there-  
79 fore their scaling parameter are extracted together by simultaneous fit. The scaling parameter  
80 is greater than 1, which indicates that their yield increase more rapidly than the increase of the  
81 number of participating nucleons. Double strange hadron production  $\Xi^-$ , it has larger scaling  
82 parameter than  $K_S^0$  and  $\Lambda$ , which indicates that  $\Xi^-$  yield increase more rapidly. This may  
83 be because  $\Xi^-$  has different production channel than  $NN \rightarrow N\Xi KK$ . The scaling parameter  
84 decrease with increasing collision energy, which show the centrality dependence of strange  
85 hadron yield weakening as collision energy increases.

86 We also compare this result with transport model UrQMD, and the UrQMD qualitatively  
87 reproduces the energy dependence, but it cannot quantitatively describe in all energies, espe-  
88 cially  $\sqrt{s_{NN}} = 7.7$  to  $11.5$  GeV for  $\Xi^-$ , which may be due to missing medium effects.

## 89 4 Summary

90 In these proceeding, we report yield measurements of  $K_S^0$ ,  $\Lambda$  and  $\Xi^-$  in Au+Au collisions at  
91  $\sqrt{s_{NN}} = 3.2, 3.5, 3.9$  and  $4.5$  GeV. Their  $dN/dy$  are presented and the strangeness excitation  
92 function are updated. The decreasing  $\alpha_S$  represent centrality dependence of yield as energy  
93 increase is shown.

94 **Acknowledgement:** This work was supported in part by the National Natural Science Foundation  
95 of China (Grant No. 12375134 and No. 12305146), the National Key Research and Development  
96 Program of China under Grant No. 2020YFE0202002, and the Fundamental Research Funds for the  
97 Central Universities (Grant No. CCNU22QN005).

## 98 References

- 99 [1] P. Koch, et.al. Physics Reports **142**, 167 (1986) 4.  
100 [2] C. Blume and C. Markert. Progress in Particle and Nuclear Physics **66**, 834 (2011) 4.  
101 [3] J.H. Chen, et.al. arXiv:2407.02935[nucl-ex].  
102 [4] F. Liu, et.al. SCIENTIA SINICA Physica, Mechanica & Astronomica **53**, 290003 (2023)  
103 9.  
104 [5] I. Kisel. Journal of Physics: Conference Series **1602**, 012006 (2020) 1.  
105 [6] STAR Collaboration. arXiv:2407.10110[nucl-ex].  
106 [7] STAR Collaboration. Physics Letters B **831**, 137152 (2022).  
107 [8] STAR Collaboration. Physics Review C **102**, 034909 (2020).  
108 [9] HADES Collaboration. Physics Letters B **793**, 457 (2019).